Front. Mech. Eng. 2016, 11(3): 289–298
DOI 10.1007/s11465-016-0393-y

RESEARCH ARTICLE

**Biranchi PANDA, A. GARG, Zhang JIAN, Akbar HEIDARZADEH, Liang GAO**

# Characterization of the tensile properties of friction stir welded aluminum alloy joints based on axial force, traverse speed, and rotational speed



**Abstract** Friction stir welding (FSW) process has gained attention in recent years because of its advantages over the conventional fusion welding process. These advantages include the absence of heat formation in the affected zone and the absence of large distortion, porosity, oxidation, and cracking. Experimental investigations are necessary to understand the physical behavior that causes the high tensile strength of welded joints of different metals and alloys. Existing literature indicates that tensile properties exhibit strong dependence on the rotational speed, traverse speed, and axial force of the tool that was used. Therefore, this study introduces the experimental procedure for measuring tensile properties, namely, ultimate tensile strength (UTS) and tensile elongation of the welded AA 7020 Al alloy. Experimental findings suggest that a welded part with high UTS can be achieved at a lower heat input compared with the high heat input condition. A numerical approach based on genetic programming is employed to produce the functional relationships between tensile properties and the three inputs (rotational speed, traverse speed, and axial force) of the FSW process. The formulated models were validated based on the experimental data, using the statistical metrics. The effect of the three inputs on the tensile properties was investigated using 2D and 3D analyses. A high UTS was achieved, including a rotational speed of 1050 r/min and traverse speed of 95 mm/min. The results also indicate that 8 kN axial force should be set prior to the FSW process.

**Keywords** tensile properties, ultimate tensile strength, tensile elongation, friction stir welding, tool rotational speed, genetic programming, welding speed

## 1 Introduction

The use of non-conventional welding such as friction stir welding (FSW) (Fig. 1) has gained attention in recent years; this method works by using a third body tool to join two facing surfaces (metals/alloys) [1–3]. Unlike conventional welding processes, FSW does not cause welding defects, such as distortion, heat-affected zone, cracking, porosity, and other defects [4–8]. Given these advantages,

Received April 16, 2016; accepted May 9, 2016

Biranchi PANDA
IDMEC, Instituto Superior Técnico, Universidade de Lisboa, Lisboa 1040-001, Portugal

A. GARG (✉), Zhang JIAN
Department of Mechatronics Engineering, Shantou University, Shantou 515063, China
E-mail: akhil@stu.edu.cn

Akbar HEIDARZADEH
Department of Materials Engineering, Azarbaijan Shahid Madani University, Tabriz, Iran

Liang GAO
The State Key Laboratory of Digital Manufacturing Equipment and Technology, Huazhong University of Science and Technology, Wuhan 430074, China

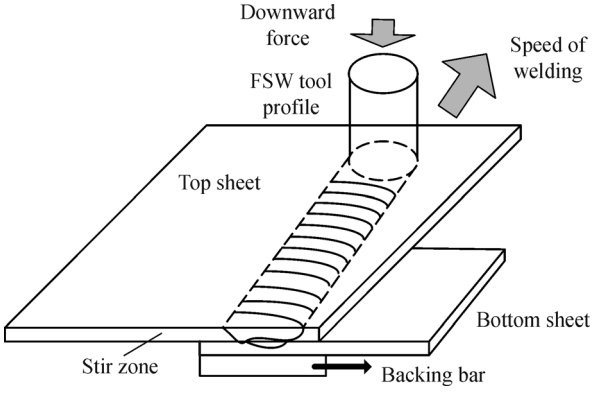


**Fig. 1** Mechanism of the FSW process at the top and bottom sheets

FSW has become a popular solid-state welding process with high tensile properties when joining two welded elements that comprise metals/alloys [9,10]. The functional performance and reliability of the final product rely on the properties of welded elements. These properties also depend on several process parameters, such as the speed of the welding process, the tool, the tool profile, and forces (axial) from the FSW process [11,12].

Literature [13–16] indicates that experiments and statistical modeling tools have been used to characterize and optimize friction stir welded metals. Several authors explored the mechanical, microstructure, and fractography properties of weldment by deploying instruments such as scanning electron microscope (SEM) [14–18]. In numerical modeling, response surface methodology (RSM) was used to determine the relation between the parameters of FSW process and to identify appropriate settings that optimize the properties of welded joints [3,13]. For instance, the properties of Al 6061-T6 alloy were evaluated, such as grain size, ultimate tensile strength (UTS), and hardness. The optimum settings of the inputs were determined using RSM [17]. Findings show that the maximum UTS of the welded joint is obtained at a rotational speed of 1100 r/min, a welding speed of 80 mm/min, and tool hardness of 45 HRC. In another study, the mechanical properties of the welded AA 2219 Al alloy were optimized using the Hooke and Jeeves methodology [18]. The mechanical properties of welded Cu plates with varying thickness were predicted and optimized by RSM using the statistical design expert platform [19]. The applied RSM methodology is based on the assumption of the model structure and subsequent identification of significant inputs using analysis of variance. The mechanism of the FSW process is complex and involves heat mechanisms [20,21]; therefore, the assumption of the model structure induces ambiguity in the extrapolation ability of the model. An alternative route is to apply advanced optimization tools [22], such as artificial neural networks and its variants [23–25], genetic programming (GP) and its variants [26,27], hybrid optimization methods of GP [28,29], and molecular dynamics [30,31]. These methods complement the limitations of RSM. Among the several optimization tools, evolutionary approach based on GP can be a potential alternative because it automatically evolves the functional expressions of process parameters [32–37]. Previous studies [38–39] have proven the ability of the applications of GP in modeling and the optimization of complex manufacturing processes.

Existing literature also suggested that Al alloys (category of 5xxx) were often used instead of steel in the marine industry because they have good corrosion resistance and lightweight properties. For materials with high mechanical strength, category 7xxx Al alloy can be used. The weldability of Al alloys is high. However, conventional welding methods result in low mechanical properties. Therefore, non-conventional FSW seems a suitable alternative. To the best of the author's knowledge, limited studies based on experimental and numerical investigation have been conducted to characterize the mechanical and microstructural properties of FSW-welded Al alloys [17,18].

This study introduces the experimental setup for the measurement of tensile properties (UTS and tensile elongation (EL)) followed by the microstructural characterization of welded AA 7020 Al alloy. To study the effect of the process parameters on tensile properties, the models are formulated (functional expressions) based on the evolutionary framework of GP. The models are validated based on experimental data using the statistical error metrics. To measure the nature of the effect of inputs on tensile properties, 2D and 3D analyses are conducted; these analyses validate the experiment discussed in Section 2. The complete procedure of the experimental and numerical investigation is shown in Fig. 2.

## 2 Experimental setup of the FSW process

The experimental study used in this work is based on Heidarzadeh et al. [40]. The material used in the experimental setup of FSW is an Al alloy (AA 7020) plate with a thickness of 4 mm and the following designated tensile properties: UTS of 400 MPa and 15% EL. The composition and microstructure of the Al alloy comprises Al (85.44%), Ti (0.08%), Zn (4.70%), Cu (0.10%), Cr (0.14%), Fe (0.35%), Mn (0.24%), Mg (1.30%), and others (7.65%).

The tool used for FSW is made of H13 steel with the following dimensions: 12 mm shoulder, cylindrical pin with a 4 mm diameter, 3.8 mm length, and 2.5° tilt against the work pieces that were used [40].

The joints were fabricated by perpendicular movement of the tool to the rolling of the plates. Varying the rotational speed of the tool ($x_1$), welding traverse speed ($x_2$), and axial force ($x_3$) (Table 1) enabled the measurement of the UTS and EL of the welded AA 7020 Al alloy. The assumptions and settings used in this study are also discussed in Ref. [40].

Data that comprise 46 samples were collected from the experimental analysis, as shown in Table 2. The variation of each data sample for UTS and EL is shown in Figs. 3(a) and 3(b). The figures clearly show that the variation of each tensile property with respect to the rotational speed, traverse speed, and axial force of the tool is highly nonlinear.

An optical microscope was used to analyze the microstructure of welded joints. The grain of the welded element is smaller when low heat is applied to the process compared with when high input is used. Fine grain size

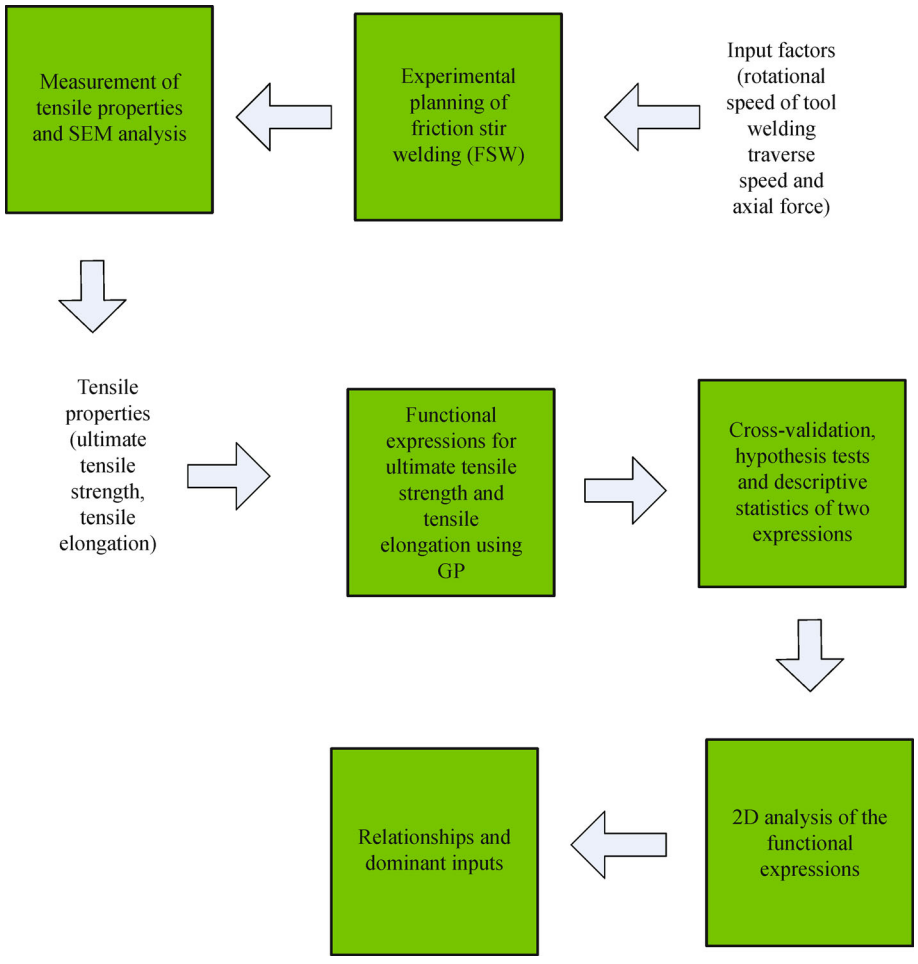


**Fig. 2** Procedure of the experimental and numerical investigation of the tensile properties of FSW-welded joints

**Table 1** Inputs used for the experimental set-up of FSW

| | $x_1$/(r·min$^{-1}$) | $x_2$/(mm·min$^{-1}$) | $x_3$/kN |
|---|---|---|---|
| Minimum | 47.00 | 58.00 | 5.32 |
| Mean | 944.69 | 94.15 | 6.76 |
| Maximum | 1200.00 | 125.00 | 8.00 |

**Table 2** Uniform experiment design for the measurement of tensile properties

| No. | $x_1$/(r·min$^{-1}$) | $x_2$/(mm·min$^{-1}$) | $x_3$/kN | UTS/MPa | EL/% |
|---|---|---|---|---|---|
| 1 | 1200 | 75 | 8.00 | 273.0508 | 7.689788 |
| 2 | 800 | 125 | 8.00 | 260.7020 | 4.634279 |
| 3 | 1200 | 125 | 8.00 | 265.2557 | 7.689788 |
| 4 | 664 | 100 | 7.00 | 243.8742 | 6.836077 |
| ⋮ | ⋮ | ⋮ | ⋮ | ⋮ | ⋮ |
| 15 | 664 | 100 | 7.00 | 243.8742 | 6.836077 |
| 16 | 1000 | 58 | 7.00 | 249.4299 | 6.018916 |

(*Continued*)

| No. | $x_1$/(r·min$^{-1}$) | $x_2$/(mm·min$^{-1}$) | $x_3$/kN | UTS/MPa | EL/% |
|---|---|---|---|---|---|
| 17 | 1000 | 58 | 7.00 | 249.4299 | 6.018916 |
| ⋮ | ⋮ | ⋮ | ⋮ | ⋮ | ⋮ |
| 39 | 900 | 100 | 8.00 | 299.2947 | 5.171500 |
| 40 | 1200 | 75 | 6.00 | 269.9894 | 7.689788 |
| 41 | 800 | 125 | 6.00 | 230.6714 | 4.634279 |
| 42 | 1200 | 125 | 6.00 | 262.1943 | 7.689788 |
| 43 | 1000 | 100 | 7.00 | 305.1451 | 6.018916 |
| 44 | 900 | 58 | 5.32 | 207.3690 | 5.171500 |
| 45 | 664 | 100 | 7.00 | 243.8742 | 6.836077 |
| 46 | 664 | 100 | 7.00 | 243.8742 | 6.836077 |

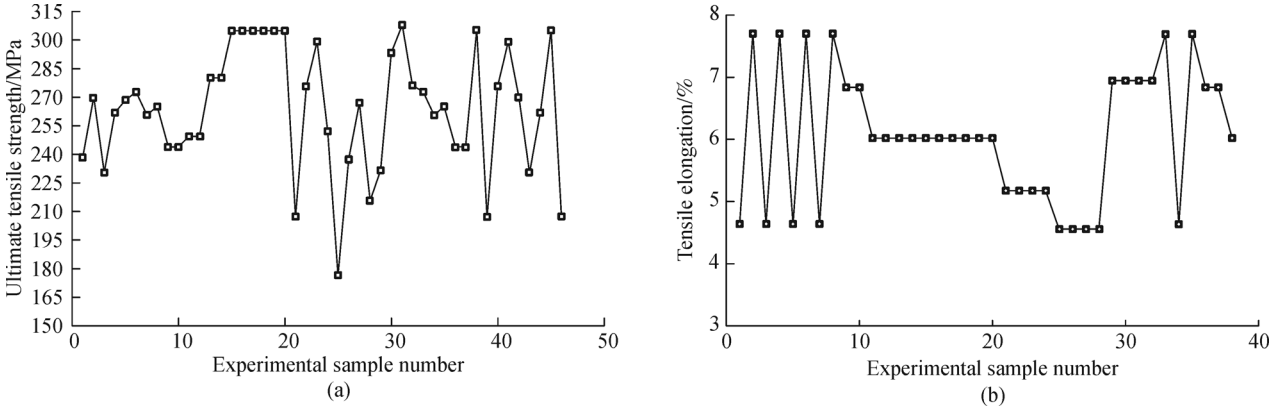


**Fig. 3** Line graph showing the nature of (a) ultimate tensile strength, and (b) tensile elongation

results in high UTS, whereas coarse grain results in low UTS [40].

The 46 samples (Table 2) are sufficient for training the GP approach. Thirty-one samples are fed into the GP framework for training and the formulation of the models for the two tensile properties, namely, UTS and tensile elongation. The remaining 15 samples are used to test the extrapolation ability of the two models.

## 3 Numerical modeling of tensile properties

A numerical approach based on evolutionary GP [41] is introduced in this study to model the FSW process. The process includes the three inputs and the two outputs. On the basis of the complex nature of the process, the algorithm can capture the hidden patterns in the process and generate the explicit functions of the two outputs. The algorithms function based on the principles of biological evolution and natural selection. The implementation (Fig. 4) of the algorithms relies extensively on the settings of the following parameters in ascending order:

1) **Functional and terminal set**: The elements in these two sets include air thematic operations and the three inputs. This study chose sets with a wide range of elements {F = (addition, multiply, subtraction, log, cosine, sin, exponential, etc.) and T = (three inputs of FSW)} to accommodate the large varieties/structures of the models.

2) **Population size**: Population size is determined based on the number of models in the initial population. This parameter is assumed constant in the entire iterations/runs. A population size of 200 is chosen in this study.

3) **Initial generation**: The generation (first) is represented by population size. The performance of the evolved models is evaluated in this stage.

4) **Objective function**: The objective function is defined to evaluate the performance of the models. The objective function used is structural risk minimization [42] because of its ability to generalize the process behavior in past studies [43].

5) **Next generation**: The models for the next generation are generated based on the objective values of the models

in first generation. These models are generated by applying certain operations, such as genetic mutation and genetic crossover; few models evolved based on reproduction. Crossover is set at a high rate of 85% followed by mutation (12%) and reproduction (3%).

6) **Iterations/runs**: This parameter comprises the number of iterations required to terminate the algorithm. One iteration/run corresponds to the total number of generations. A total of 20 iterations are computed in this study.

Simulations are performed in MATLAB (2010b) based on the GPTIPS box developed by Searson et al. [44]. The best GP models (Eqs. (A1) and (A2) in the Appendix) for the two tensile properties are selected based on the minimum mean absolute percentage error (MAPE) value in all runs. Experimental validation with 2D and 3D analyses is discussed in Section 4.

$$\mathrm{MAPE} = \frac{1}{n}\sum_{i}\left|\frac{A_i - M_i}{A_i}\right| \times 100\%, \tag{1}$$

where $A_i$ is the actual value, $M_i$ is the predicted value from the model, and $n$ is the number of training samples.

## 4 Performance analysis of UTS and EL models

The models are statistically evaluated using three metrics, namely, coefficient of determination ($R^2$), root mean square error (RMSE), and MAPE. These metrics reflect the deviations of the actual values from the predicted values. The mathematical representation of these metrics is provided in Vijayaraghavan et al. [35]. Table 3 shows that the values for $R^2$, RMSE, and MAPE are low for the GP models in the training and testing data sets for the two tensile properties (UTS and EL). Table 4 and Fig. 5 show that the actual values and the numerical values of the GP models are close with great accuracy. Thus, the analysis indicates that the GP models can be used to accurately generalize the FSW outputs with low deviation values.

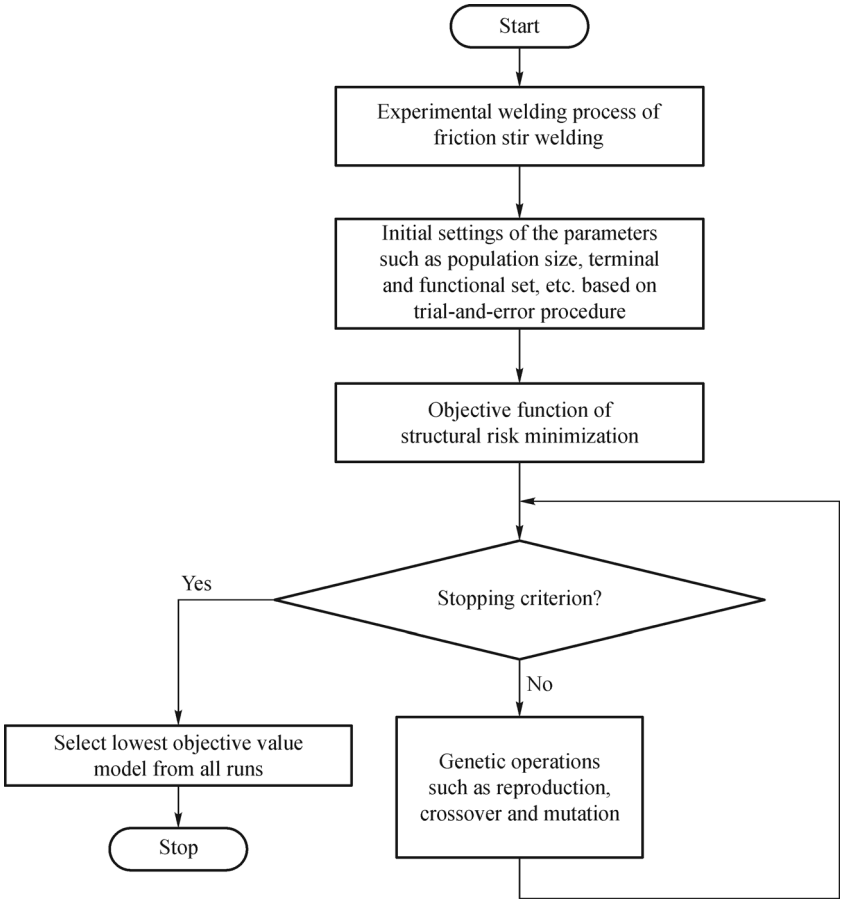


**Fig. 4** GP approach for modeling tensile properties

**Table 3** Statistical metrics of the models for two tensile properties

| Models | $R^2$ | | RMSE/% | | MAPE/% | |
|---|---|---|---|---|---|---|
| | Training phase | Testing phase | Training phase | Testing phase | Training phase | Testing phase |
| GP (UTS) | 0.98 | 0.96 | 1.31 | 1.91 | 0.39 | 0.60 |
| GP (EL) | 0.97 | 0.96 | 0.42 | 0.45 | 0.73 | 0.81 |

**Table 4** Actual and model values for two tensile properties obtained from the models

| No. | Actual UTS /MPa | Predicted UTS /MPa | Actual EL/% | Predicted EL/% |
|---|---|---|---|---|
| 1 | 276.5059 | 274.8061 | 6.943182 | 6.943139 |
| 2 | 273.0508 | 273.2518 | 7.689788 | 7.689746 |
| 3 | 260.7020 | 261.8811 | 4.634279 | 4.634237 |
| 4 | 265.2557 | 267.1045 | 7.689788 | 7.689746 |
| 5 | 243.8742 | 243.0871 | 6.836077 | 6.836035 |
| 6 | 243.8742 | 243.0871 | 6.836077 | 6.836035 |
| 7 | 305.1451 | 305.2267 | 6.018916 | 6.018874 |
| 8 | 207.3690 | 211.4123 | 5.171500 | 5.171457 |
| 9 | 275.9505 | 275.0003 | 5.171500 | 5.171457 |
| 10 | 299.2947 | 297.4679 | 5.171500 | 5.171457 |
| 11 | 269.9894 | 268.1412 | 7.689788 | 7.689746 |
| 12 | 230.6714 | 232.8499 | 4.634279 | 4.634237 |
| 13 | 262.1943 | 261.9938 | 7.689788 | 7.689746 |
| 14 | 305.1451 | 305.2267 | 6.018916 | 6.018874 |
| 15 | 207.3690 | 211.4123 | 5.171500 | 5.171457 |

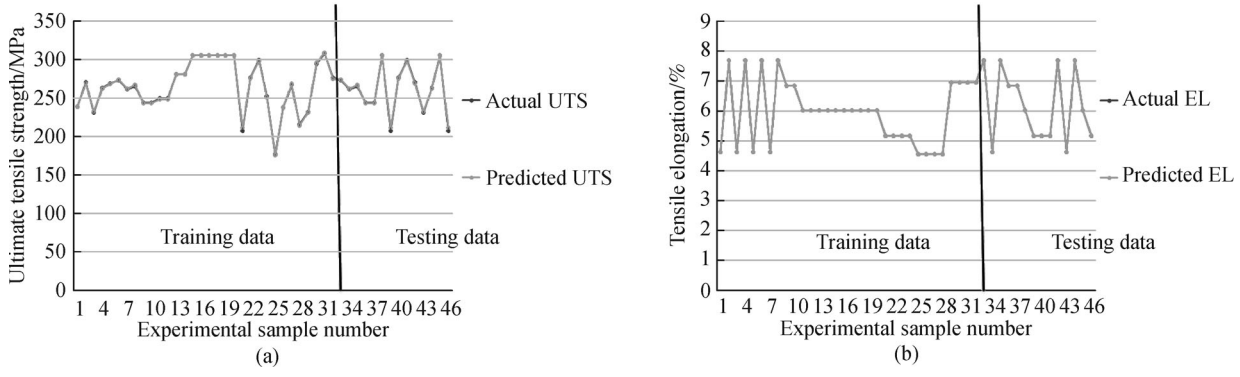


**Fig. 5** Curve fitting of the tensile properties models on the data set. (a) Ultimate tensile strength; (b) tensile elongation

## 5 2D and 3D surface analyses for the proposed models

Surface analysis is performed based on the parametric and sensitivity analysis of the two GP models (UTS and EL). Details of the procedures for analysis are given in Garg et al. [43]. The main effects of each input on the tensile properties of the GP models are estimated using 2D analysis. As shown in Fig. 6(a), 2D analysis demonstrates that UTS increases linearly with the increased rotational speed values of the tool to a certain point before it starts to decrease. The behavior of UTS with respect to traverse speed is similar to that of the rotational speed of the tool (Fig. 6(b)). The UTS of the welded Al alloy element increases nonlinearly with an increase in axial force value (Fig. 6(c)). The effect of axial force on the EL of welded Al

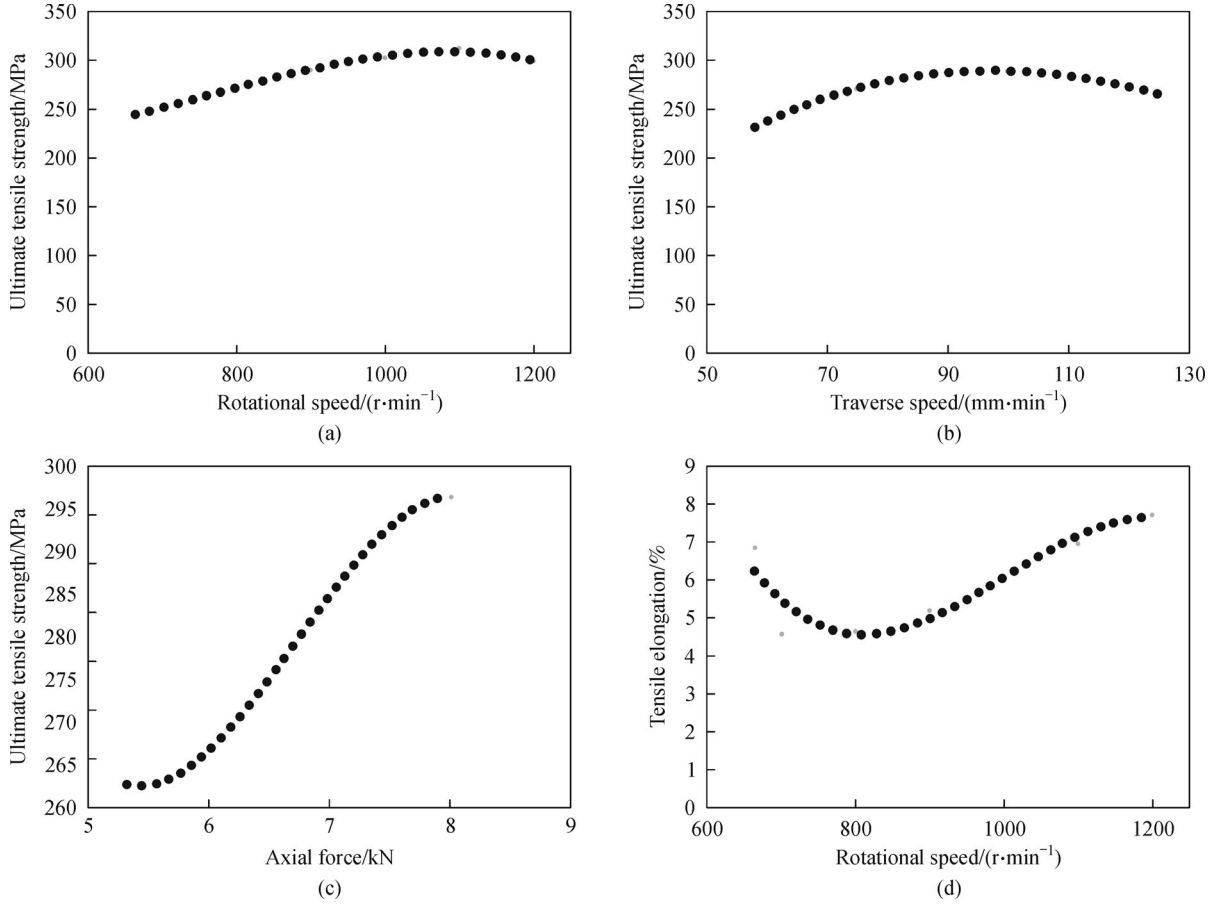


**Fig. 6** 2D plots showing the relationships of (a) ultimate tensile strength and rotational speed, (b) ultimate tensile strength and traverse speed, (c) ultimate tensile strength and axial force, and (d) tensile elongation and rotational speed

alloy element was hardly noticed, as shown in Fig. 6(d). With respect to rotational speed, EL initially decreases to a certain point and then increases. The effect of the interaction between the two inputs on two tensile properties is estimated using 3D analysis. The 3D surface plots (Fig. 7) show the combined effect of inputs (rotational speed and traverse speed, traverse speed and axial force, rotational speed and axial force) on the UTS of the welded Al alloy joints. Similarly, Fig. 8 shows the combined effect of inputs (rotational speed and axial force, rotational speed and traverse speed) on the EL of the welded Al alloy joints. Sensitivity analysis (Fig. 9) is conducted based on parametric analysis. The sensitivity of each input is determined by calculating the maximum and minimum in the 2D and 3D plots. Figures 9(a) and 9(b) show that the rotational speed of the tool has the strongest influence on UTS and EL. UTS is arranged according to rotational speed followed by traverse speed and axial force. Axial force and traverse speed have no effect on EL. These plots show that achieving a high UTS requires a rotational speed of 1050 r/min, a traverse speed of 95 mm/min, and an axial force of 8 kN, which should be set prior to the FSW process.

## 6 Conclusions

Experimental procedure and microscopic characterization are conducted in this study to measure the tensile properties (UTS and EL) of Al alloy (AA 7020) joints welded through FSW. Experimental findings suggest that a high UTS for the welded part of Al alloy (AA 7020) can be achieved at a low heat input condition than at a high heat input condition. An optimization framework based on GP is used to produce the functional expressions of the two tensile properties. Performance analysis of the GP models based on statistical error metrics suggests that the models can extrapolate the UTS and EL values beyond the given

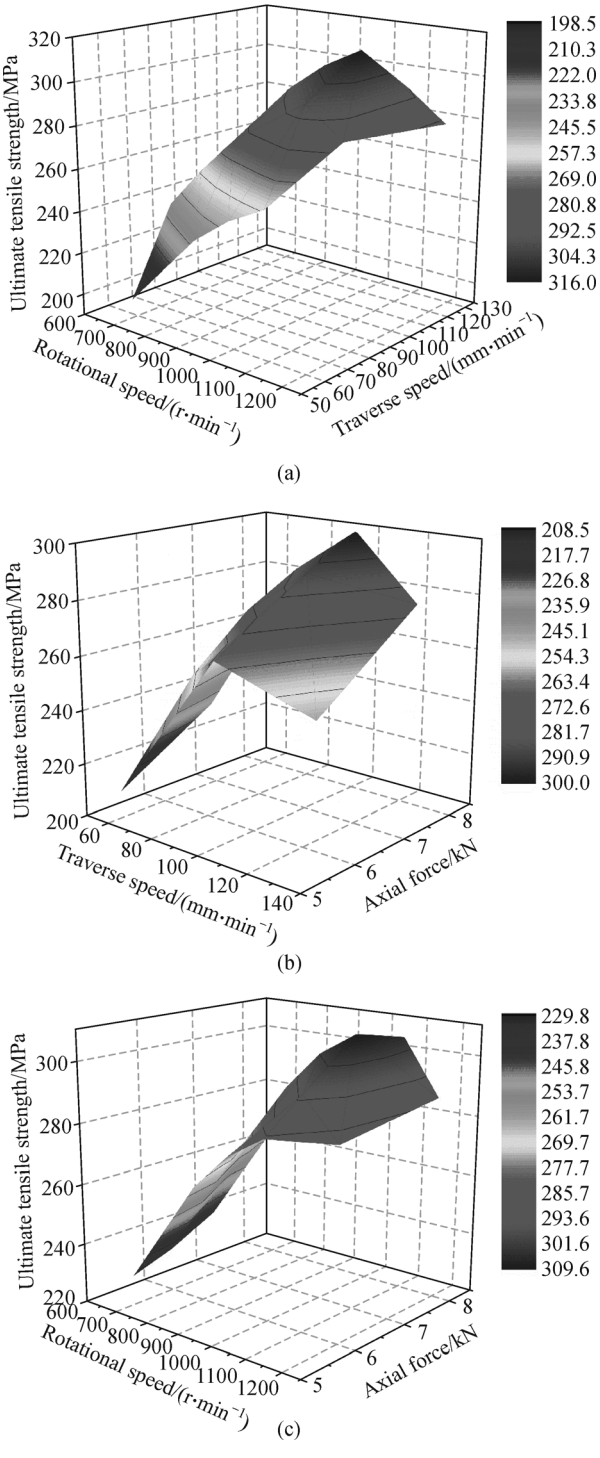


**Fig. 7** 3D plots showing the relationships of ultimate tensile strength and (a) rotational speed and traverse speed, (b) traverse speed and axial force, and (c) rotational speed and axial force

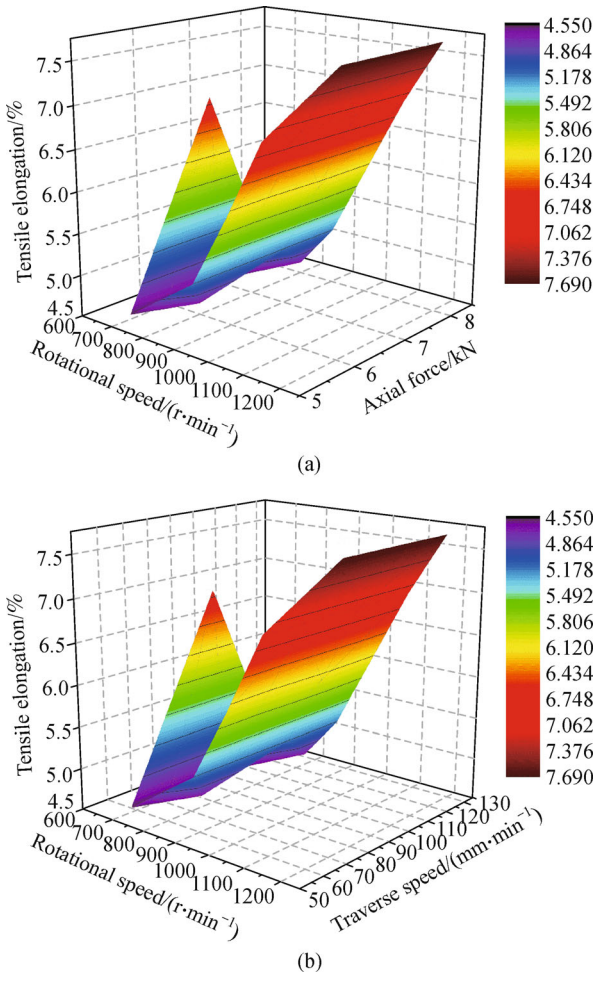


**Fig. 8** 3D plots showing the relationships of tensile elongation based on (a) rotational speed and axial force, (b) rotational speed and traverse speed

range of inputs (axial force, rotational speed, and traverse speed). The functional expressions can be used offline to accurately determine the tensile properties of the welded part of Al alloy. The model analysis shows that the dominant input for achieving high UTS and EL is the rotational speed of the tool. EL initially decrease and then increase with an increase in the rotational speed values of the tool. Parametric procedure based on the 2D and 3D plot analyses shows a high nonlinear interaction effect between the rotational speed and traverse speed on the two tensile properties. Future work should include additional parameters, such as tool pin profile, shoulder diameter, and tool hardness. Future work should also investigate the effect of these parameters on the two tensile properties of the welded part of the Al alloy to evaluate any differences from this study.

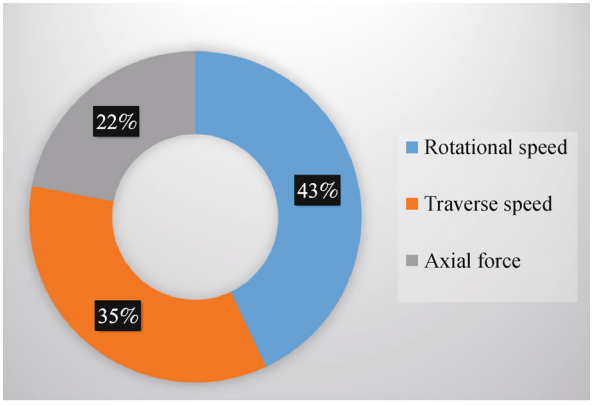


(a)

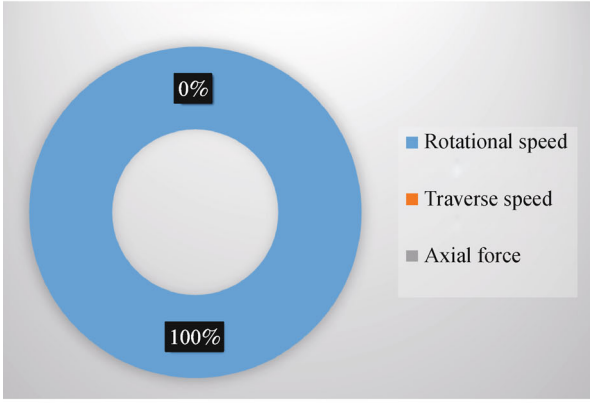


(b)

**Fig. 9** Percentage contribution of the three inputs to (a) ultimate tensile strength, and (b) tensile elongation

**Acknowledgements** This study was supported by Shantou University Scientific Research Funded Project (Grant No. NTF 16002).

## References

1. Yazdipour A, Heidarzadeh A. Effect of friction stir welding on microstructure and mechanical properties of dissimilar Al 5083-H321 and 316L stainless steel alloy joints. Journal of Alloys and Compounds, 2016, 680: 595–603
2. Yazdipour A, Heidarzadeh A. Dissimilar butt friction stir welding of Al 5083-H321 and 316L stainless steel alloys. The International Journal of Advanced Manufacturing Technology, 2016, 1–8
3. Heidarzadeh A, Khodaverdizadeh H, Mahmoudi A, et al. Tensile behavior of friction stir welded AA 6061-T4 aluminum alloy joints. Materials & Design, 2012, 37: 166–173
4. Heidarzadeh A, Kazemi-Choobi K, Hanifian H, et al. 3-Microstructural evolution. In: Besharati-Givi M K, Asadi P, eds. Advances in Friction-Stir Welding and Processing. Woodhead Publishing, 2014, 65–140
5. Khodaverdizadeh H, Mahmoudi A, Heidarzadeh A, et al. Effect of friction stir welding (FSW) parameters on strain hardening behavior of pure copper joints. Materials & Design, 2012, 35: 330–334
6. Heidarzadeh A, Saeid T. A comparative study of microstructure and mechanical properties between friction stir welded single and double phase brass alloys. Materials Science and Engineering A, 2016, 649: 349–358
7. Heidarzadeh A, Saeid T. On the effect of β phase on the microstructure and mechanical properties of friction stir welded commercial brass alloys. Data in Brief, 2015, 5: 1022–1025
8. Heidarzadeh A, Saeid T. Correlation between process parameters, grain size and hardness of friction-stir-welded Cu-Zn alloys. Rare Metals, 2016, 1–11
9. Heidarzadeh A, Jabbari M, Esmaily M. Prediction of grain size and mechanical properties in friction stir welded pure copper joints using a thermal model. The International Journal of Advanced Manufacturing Technology, 2015, 77(9–12): 1819–1829
10. Golezani A S, Barenji R V, Heidarzadeh A, et al. Elucidating of tool rotational speed in friction stir welding of 7020-T6 aluminum alloy. International Journal of Advanced Manufacturing Technology, 2015, 81(5–8): 1155–1164
11. Rahimzadeh Ilkhichi A, Soufi R, Hussain G, et al. Establishing mathematical models to predict grain size and hardness of the friction stir-welded AA 7020 aluminum alloy joints. Metallurgical and Materials Transactions B, 2015, 46 (1): 357–365
12. Barenji R V. Influence of heat input conditions on microstructure evolution and mechanical properties of friction stir welded pure copper joints. Transactions of the Indian Institute of Metals, 2016, 69(5): 1077–1085
13. Garg A, Panda B, Shankhwar K. Investigation of the joint length of weldment of environmental-friendly magnetic pulse welding process. The International Journal of Advanced Manufacturing Technology, 2016, 1–12
14. Barenji R V. Effect of tool traverse speed on microstructure and mechanical performance of friction stir welded 7020 aluminum alloy. Proceedings of the Institution of Mechanical Engineers, Part L: Journal of Materials Design and Applications, 2015, 230(2): 1–11
15. Azizi A, Barenji R V, Barenji A V, et al. Microstructure and mechanical properties of friction stir welded thick pure copper plates. The International Journal of Advanced Manufacturing Technology, 2016, 1–11
16. Sharma V, Prakash U, Kumar B M. Surface composites by friction stir processing: A review. Journal of Materials Processing Technology, 2015, 224: 117–134
17. Rajakumar S, Muralidharan C, Balasubramanian V. Establishing empirical relationships to predict grain size and tensile strength of friction stir welded AA 6061-T6 aluminium alloy joints. Transactions of Nonferrous Metals Society of China, 2010, 20(10): 1863–1872
18. Babu S, Elangovan K, Balasubramanian V, et al. Optimizing friction stir welding parameters to maximize tensile strength of AA2219 aluminum alloy joints. Metals and Materials International, 2009, 15 (2): 321–330
19. Heidarzadeh A, Saeid T, Khodaverdizadeh H, et al. Establishing a mathematical model to predict the tensile strength of friction stir welded pure copper joints. Metallurgical and Materials Transactions B, Process Metallurgy and Materials Processing Science, 2013, 44 (1): 175–183

20. Lakshminarayanan A K, Balasubramanian V. Comparison of RSM with ANN in predicting tensile strength of friction stir welded AA7039 aluminium alloy joints. Transactions of Nonferrous Metals Society of China, 2009, 19(1): 9–18
21. Mohammadzadeh A, Azadbeh M, Namini S A. Densification and volumetric change during supersolidus liquid phase sintering of prealloyed brass Cu28Zn powder: modeling and optimization. Science of Sintering, 2014, 46(1): 23–35
22. Zhao D, Tian Q, Li Z, et al. A new stepwise and piecewise optimization approach for CO 2 pipeline. International Journal of Greenhouse Gas Control, 2016, 49: 192–200
23. Zhao D, Zhu Q, Dubbeldam J. Terminal sliding mode control for continuous stirred tank reactor. Chemical Engineering Research & Design, 2015, 94: 266–274
24. Zhao D, Ni W, Zhu Q. A framework of neural networks based consensus control for multiple robotic manipulators. Neurocomputing, 2014, 140: 8–18
25. Zhao D, Zhu Q, Li N, et al. Synchronized control with neuro-agents for leader—Follower based multiple robotic manipulators. Neurocomputing, 2014, 124: 149–161
26. Vijayaraghavan V, Garg A, Wong C H, et al. An integrated computational approach for determining the elastic properties of boron nitride nanotubes. International Journal of Mechanics and Materials in Design, 2015, 11(1): 1–14
27. Vijayaraghavan V, Castagne S. Computational model for predicting the effect of process parameters on surface characteristics of mass finished components. Engineering Computations, 2016, 33(3): 789–805
28. Garg A, Vijayaraghavan V, Wong C H, et al. Combined CI-MD approach in formulation of engineering moduli of single layer graphene sheet. Simulation Modelling Practice and Theory, 2014, 48: 93–111
29. Vijayaraghavan V, Castagne S. Sustainable manufacturing models for mass finishing process. The International Journal of Advanced Manufacturing Technology, 2015, 1–9
30. Vijayaraghavan V, Wong C H. Torsional characteristics of single walled carbon nanotube with water interactions by using molecular dynamics simulation. Nano-Micro Letters, 2014, 6(3): 268–279
31. Wong C H, Vijayaraghavan V. Nanomechanics of imperfectly straight single walled carbon nanotubes under axial compression by using molecular dynamics simulation. Computational Materials Science, 2012, 53(1): 268–277
32. Panda B N, Bahubalendruni M R, Biswal B B. A general regression neural network approach for the evaluation of compressive strength of FDM prototypes. Neural Computing & Applications, 2015, 26 (5): 1129–1136
33. Panda B N, Bahubalendruni M R, Biswal B B. Comparative evaluation of optimization algorithms at training of genetic programming for tensile strength prediction of FDM processed part. Procedia Materials Science, 2014, 5: 2250–2257
34. Panda B N, Babhubalendruni M R, Biswal B B, et al. Application of artificial intelligence methods to spot welding of commercial aluminum sheets (B.S. 1050). In: Das K N, Deep K, Pant M, et al. eds. Proceedings of Fourth International Conference on Soft Computing for Problem Solving. Springer, 2015, 21–32
35. Vijayaraghavan V, Garg A, Lam J S L, et al. Process characterisation of 3D-printed FDM components using improved evolutionary computational approach. International Journal of Advanced Manufacturing Technology, 2015, 78(5–8): 781–793
36. Garg A, Vijayaraghavan V, Wong C H, et al. An embedded simulation approach for modeling the thermal conductivity of 2D nanoscale material. Simulation Modelling Practice and Theory, 2014, 44: 1–13
37. Garg A, Tai K. Comparison of regression analysis, artificial neural network and genetic programming in handling the multicollinearity problem. In: Proceedings of 2012 International Conference on Modelling, Identification & Control (ICMIC). Wuhan: IEEE, 2012, 353–358
38. Asghari A, Gandomi A H. Ductility reduction factor and collapse mechanism evaluation of a new steel knee braced frame. Structure and Infrastructure Engineering: Maintenance, Management, Life-Cycle Design and Performance, 2016, 12(2): 239–255
39. Gandomi A H, Faramarzifar A, Rezaee P G, et al. New design equations for elastic modulus of concrete using multi expression programming. Journal of Civil Engineering and Management, 2015, 21(6): 761–774
40. Heidarzadeh A, Barenji R V, Esmaily M, et al. Tensile properties of friction stir welds of AA 7020 aluminum alloy. Transactions of the Indian Institute of Metals, 2015, 68(5): 757–767
41. Koza J R. Genetic Programming: On the Programming of Computers by Means of Natural Selection. Cambridge: MIT press, 1992
42. Vapnik V N. Statistical Learning Theory. New York: Wiley, 1998
43. Garg A, Lam J S L, Gao L. Energy conservation in manufacturing operations: Modelling the milling process by a new complexity-based evolutionary approach. Journal of Cleaner Production, 2015, 108: 34–45
44. Searson D P, Leahy D E, Willis M J. GPTIPS: An open source genetic programming toolbox for multigene symbolic regression. In: Proceedings of the International MultiConference of Engineers and Computer Scientists. Hong Kong: Newswood Ltd., 2010, 1: 77–80

## Appendix:

$$\text{Ultimate tensile strength}_{GP} = 89.187 + 0.51586\times[x_2 - \sin(\tan(x_1 + x_3))] + 12.8573\times\sin[x_1 + \cos(\exp(\text{plog}(x_3)))] + \tanh[\tanh(\sin(-9.354553\times\sin x_3))] + 8.3616\times\text{plog}(\sin x_1) + 20.7737\times\sin x_3 - 27.0493\times\sin(\exp(x_2)) - 4.009\times\tan(\text{plog}(\sin x_1)) + 0.1097\times x_1 \quad \text{(A1)}$$

$$\text{Tensile elongation}_{GP} = 0.057974 + 0.057974\times\tanh x_2 - 0.046896\times\cos 2.513109 + 0\times\text{plog}(\tanh x_2) - 1.2146\times(\sin x_1 - \tanh x_1) + 0.53143\times 9.166777 + 1.2896\times\cos x_1 + 0.057974\times\tanh x_2 \quad \text{(A2)}$$